5

Vision-Based Control of the Mechatronic System

Rong-Fong Fung[1] and Kun-Yung Chen[2]
[1]*Department of Mechanical and Automation Engineering*
[2]*Institute of Engineering Science and Technology*
National Kaohsiung First University of Science and Technology
1 University Road, Yenchau, Kaohsiung County 824,
Taiwan

1. Introduction

The mechatronic system is employed widely in the industry, transportation, aviation and military. The system consists of an electrical actuator and a mechanism, and commonly is effective in industry territory. The toggle mechanism has many applications where overcome a large resistance with a small driving force is necessary; for examples, clutches, rock crushers, truck tailgates, vacuum circuit breakers, pneumatic riveters, punching machines, forging machines and injection modeling machines, etc. The motion controls of the motor-toggle mechanism have been studied (Lin *et al.*, 1997; Fung & Yang, 2001; Fung *et al.*, 2001). (Lin *et al.1997)* proposed a fuzzy logic controller, which was based on the concept of hitting condition without using the complex mathematical model for a motor-mechanism system. The fuzzy neural network controller (Wai *et al.*, 2001; Wai, 2003) was applied to control a motor-toggle servomechanism. The numerical results via the inverse dynamics control and variable structure control (VSC) were compared for an electrohydraulic actuated toggle mechanism (Fung & Yang, 2001). The VSC (Fung *et al.*, 2001) was employed to a toggle mechanism, which was driven by a linear synchronous motor and the joint coulomb friction was considered. In the previous studies, the motion controller for the toggle mechanism had been performed extensively. But the controllers are still difficult to realize if the linear scales can not be installed in the toggle mechanism for real feedbacks of positions and speeds.

In the adaptive control territory, (Li *et al.* 2004) proposed a hybrid control scheme for the flexible structures to obtain both dynamic and static characteristics. A nonlinear strategy is proposed by (Beji & Bestaoui, 2005) to ensure the vehicle control, in which the proof of main results is based on the Lyapunov concept. In these studies, the linear scale or encoder was employed as the sensor to feedback the positions and speeds. If the sensor is difficult to install, the non-contact measure vision-based is necessary and effective to apply in the mechatronic system.

In such motor-mechanism coupled systems, the non-contact machine vision exhibits its merits to measure the output responses of the machine. In previous references (Petrovic & Brezak, 2002; Yong et al., 2001), the machine vision was implemented with the PI and PD controllers, but didn't concern about the robustness of the vision system associated with

Source: Visual Servoing, Book edited by: Rong-Fong Fung,
ISBN 978-953-307-095-7, pp. 234, April 2010, INTECH, Croatia, downloaded from SCIYO.COM

controllers. (Park & Lee, 2002) presented the visual servo control for a ball on a plate and tracked its desired trajectory by the SMC. But there was no comparison with any other controller, and the mathematical equations of motion must be exactly obtained first, then the SMC can be implemented. (Petrovic & Brezak, 2002) applied the vision systems to motion control, in which the hard real-time constrains was put on image processing and was suitable for real-time angle measurement. In the autonomous vehicle (Yong *et al.*, 2001), the reference lane was continually detected by machine vision system in order to cope with the steering delay and the side-slip of vehicle, and the PI controller was employed for the yaw rate feedback. (Nasisi & Carelli, 2003) designed the adaptive controllers for the robot's positioning and tracking by use of direct visual feedback with camera-in-hand configurations. In these previous studies, they did not either discuss about the robustness of the vision system associated with the controllers or investigate robustness performances of the controllers for robot systems in experimental realization.

The control techniques are essential to provide a stable and robust performance for a wide range of applications, e.g. robot control, process control, etc., and most of the applications are inherently nonlinear. Moreover, there exist relatively little general theories for the adaptive controls (Astrom & Wittenmark, 1995; Slotine & Li, 1991) of nonlinear systems. As the application of a motor-toggle mechanism has similar control problems to the robotic systems, the adaptive control technique developed by (Slotine and Li, 1988, 1989), which exploited the conservation of energy formulation to design control laws for the fixed position control problem, is adopted to control the motor-toggle mechanism in this chapter. The techniques made use of matrix properties of a skew-symmetric system so that the measurements of acceleration signals and the computations of inverse of the inertia matrix are not necessary. Moreover, an inertia-related Lyapunov function containing a quadratic form of a linear combination of speed- and position-error states will be formulated. Furthermore, the SMC, PD-type FLC (Rahbari & Silva, 2000) and PI-type FLC (Aracil & Gordillo, 2004) are proposed to positioning controls, and their performances by machine vision are compared between numerical simulations and experimental experiments.

In this chapter, the machine vision system is used as the sensor to measure the output state of the motor-toggle mechanism in real operational conditions. The shape-pattern and color-pattern (Hashimoto & Tomiie, 1999) on the link and slider are applied as the output objects to measure by the machine vision system. The main advantage of a vision-based measuring system is its non-contact measurement principle, which is important in cases when the contact measurements are difficult to implement.

In the theoretical analysis, Hamilton's principle, Lagrange multiplier, geometric constraints and partitioning method are employed to derive the dynamic equations. In order to control the motor-mechanism system with robust characteristics, the SMC is designed to control the slider position. However, the general problem encountered in the design of a SMC system is that the bound of uncertainties and the exact mathematical mode of the motor-mechanism system are difficult to obtain in practical applications. In order to overcome the difficulties, the PI-type FLC, which is based on the concept of hitting conditions and without using the complex mathematical model of the motor-mechanism system, is successfully proposed by machine vision numerically and experimentally.

This chapter is organized as follows. After an introduction in Section 1, a mathematical modeling is in Section 2. Section 3 shows the design of the vision-based controller. Section 4 is the numerical simulations. The machine-vision experiments are in Section 5. Finally, experimental results and conclusions are shown in Section 6 and 7, respectively.

2. Mathematical modeling of the mechatronic system

In this chapter, the motor-toggle mechanism is a representative mechatronic system and consists of a servo motor and a toggle mechanism. The electric power is transferred to mechanical power by the motor. This is the basic goal of the mechatronic system.

2.1 Mathematical model of the motor-toggle mechanism

The toggle mechanism driven by a PMSM is shown in Fig. 1(a) and its experimental equipment is shown in Fig. 1(b). The screw is a media that makes the small torque τ to convert into the large force F_C acting on the slider *C*. The conversion relationship is

$$\tau = \frac{F_C l_d}{2\pi n}, \tag{1}$$

where l_d is the lead of screw, n is the gear ratio number. (Huang et al., 2008) have shown the holomonic constraint equation for the toggle mechanism as follows:

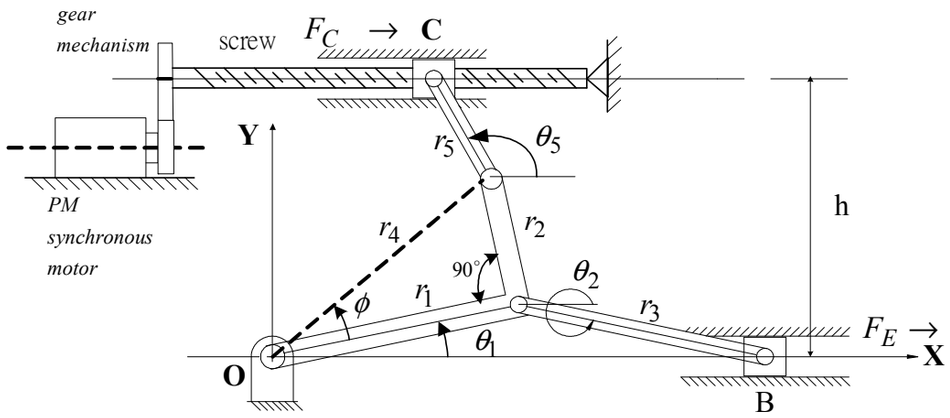

(a)

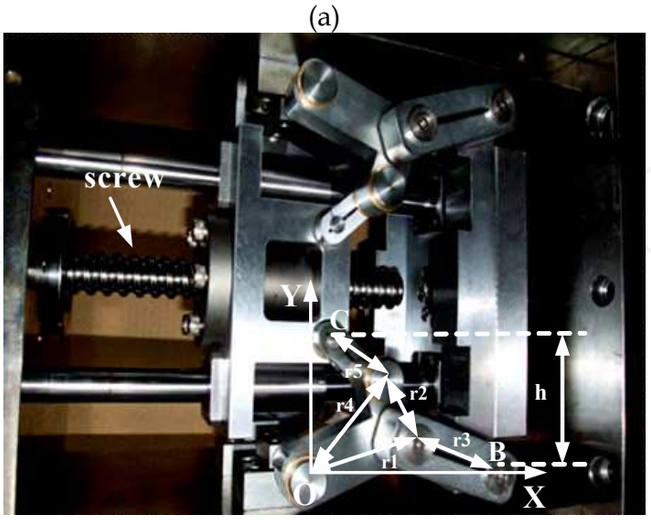

(b)

Fig. 1. The toggle mechanism driven by a PMSM. (a) The physical model. (b) The experimental equipment.

$$\mathbf{\Phi}(\boldsymbol{\theta}) = \begin{bmatrix} r_3 \sin\theta_2 + r_1 \sin\theta_1 \\ r_5 \sin(\pi - \theta_5) + r_4 \sin(\theta_2 + \phi) - h \end{bmatrix} = 0, \tag{2}$$

where $\boldsymbol{\theta} = \begin{bmatrix} \theta_5 & \theta_2 & \theta_1 \end{bmatrix}^{\mathrm{T}}$ is the vector of generalized coordinates. Similar to the previous study (Chuang et al. 2008) one obtains Euler-Lagrange equation of motion, accounting for both the applied and constraint forces, as

$$\mathbf{M}(\boldsymbol{\theta})\ddot{\boldsymbol{\theta}} + \mathbf{N}(\boldsymbol{\theta}, \dot{\boldsymbol{\theta}}) - \mathbf{B}U - \mathbf{D} + \mathbf{\Phi}_{\boldsymbol{\theta}}^{\mathrm{T}} \lambda = 0, \tag{3}$$

and the details of $\mathbf{M}$, $\mathbf{N}$, $\mathbf{B}$, U and $\mathbf{D}$ can also be found in (Chuang et al. 2008) . Taking the first and second derivatives of the constraint position Equation (2), we obtain

$$\mathbf{\Phi}_{\boldsymbol{\theta}} \dot{\boldsymbol{\theta}} = \begin{bmatrix} r_3 \dot{\theta}_2 \cos\theta_2 + r_1 \dot{\theta}_1 \cos\theta_1 \\ r_5 \dot{\theta}_5 \cos\theta_5 + r_4 \dot{\theta}_1 \cos(\theta_1 + \phi) \end{bmatrix} = 0, \tag{4}$$

$$\mathbf{\Phi}_{\boldsymbol{\theta}} \ddot{\boldsymbol{\theta}} = -(\mathbf{\Phi}_{\boldsymbol{\theta}} \dot{\boldsymbol{\theta}})_{\boldsymbol{\theta}} \dot{\boldsymbol{\theta}} = \boldsymbol{\gamma} = \begin{bmatrix} r_3 \dot{\theta}_2^2 \sin\theta_2 + r_1 \dot{\theta}_1^2 \sin\theta_1 \\ r_5 \dot{\theta}_5^2 \sin\theta_5 + r_4 \dot{\theta}_1^2 \sin(\theta_1 + \phi) \end{bmatrix} = 0. \tag{5}$$

By using these equations and Euler-Lagrange Eq. (3), we obtain the equation in the matrix form as

$$\begin{bmatrix} \mathbf{M} & \mathbf{\Phi}_{\boldsymbol{\theta}}^{\mathrm{T}} \\ \mathbf{\Phi}_{\boldsymbol{\theta}} & \mathbf{0} \end{bmatrix} \begin{bmatrix} \ddot{\boldsymbol{\theta}} \\ \lambda \end{bmatrix} = \begin{bmatrix} \mathbf{B}U + \mathbf{D}(\boldsymbol{\theta}) - \mathbf{N}(\boldsymbol{\theta}, \dot{\boldsymbol{\theta}}) \\ \boldsymbol{\gamma} \end{bmatrix}. \tag{6}$$

This is a system of differential-algebraic equations.

2.2 Reduce formulation of the differential equations

The motion equations of the toggle mechanism are summarized in the matrix form of Eq. (6) and the constraint equation (2). The following implicit method is employed to reduce the system equations.

Equations (2) and (6) may be reordered and partitioned according to the decomposition of $\boldsymbol{\theta} = \begin{bmatrix} \theta_5 & \theta_2 & \theta_1 \end{bmatrix}^T = \begin{bmatrix} \mathbf{u}^T & v^T \end{bmatrix}^T$. Thus, equation (6) can be written in the matrix form as:

$$\hat{M}(v)\ddot{v} + \hat{N}(v, \dot{v}) = \hat{Q}U + \hat{D}. \tag{7}$$

where

$$\hat{M} = M^{vv} - \mathbf{M}^{\mathbf{vu}} \mathbf{\Phi}_{\mathbf{u}}^{-1} \mathbf{\Phi}_{\mathbf{v}} - \mathbf{\Phi}_{\mathbf{v}}^{\mathbf{T}} \left(\mathbf{\Phi}_{\mathbf{u}}^{-1} \right)^{\mathbf{T}} \left[\mathbf{M}^{\mathbf{uv}} - \mathbf{M}^{\mathbf{uu}} \mathbf{\Phi}_{\mathbf{u}}^{-1} \mathbf{\Phi}_{\mathbf{v}} \right],$$

$$\hat{N} = \left[N^v - \mathbf{\Phi}_{\mathbf{v}}^{\mathbf{T}} \left(\mathbf{\Phi}_{\mathbf{u}}^{-1} \right)^{\mathbf{T}} \mathbf{N}^{\mathbf{u}} \right] + \left[\mathbf{M}^{\mathbf{vu}} \mathbf{\Phi}_{\mathbf{u}}^{-1} - \mathbf{\Phi}_{\mathbf{v}}^{\mathbf{T}} \left(\mathbf{\Phi}_{\mathbf{u}}^{-1} \right)^{\mathbf{T}} \mathbf{M}^{\mathbf{uu}} \mathbf{\Phi}_{\mathbf{u}}^{-1} \right] \boldsymbol{\gamma},$$

$$\hat{Q} = B^v - \mathbf{\Phi}_v^T \left(\mathbf{\Phi}_u^{-1} \right)^T \mathbf{B}^u, \quad U = \left[i_q^* \right], \quad \hat{D} = D^v - \mathbf{\Phi}_v^T \left(\mathbf{\Phi}_u^{-1} \right)^T \mathbf{D}^{\mathbf{u}}.$$

The elements of the vectors $\boldsymbol{u}$, v and matrices $\mathbf{\Phi_u}$, $\mathbf{\Phi_v}$, $\mathbf{M^{uu}}$, $\mathbf{M^{uv}}$, $\mathbf{M^{vu}}$, M^{vv}, $\mathbf{N^u}$ and N^v are detailed in (Huang et al., 2008) . The resultant equation (7) is a differential equation with only one independent generalized coordinate v , which is the rotation angle θ_1 of link 1 in Fig. 1(a). The system becomes an initial value problem and can be integrated by using the fourth-order Runge-Kutta method.

2.3 Field-oriented PMSM

A machine model (Lee *et al.*, 2005) of a PMSM can be described in a rotating rotor and the electric torque equation for the motor dynamics is

$$\tau_e = \tau_m + B_m\omega_r + J_m\dot{\omega}_r. \tag{8}$$

where τ_m is the load torque, B_m is the damping coefficient, ω_r is the rotor speed and J_m is the moment of inertia.

With the implementation of field-oriented control, the PMSM drive system can be simplified to a control system block diagram as shown in Fig. 2, in which

$$\tau_e = K_t i_q^*, \tag{9}$$

$$K_t = \frac{3}{2}PL_{md}I_{fd}, \tag{10}$$

$$H_p(s) = \frac{1}{J_m s + B_m}, \tag{11}$$

where i_q^* is the torque current command. By substituting (9) into (8), the applied torque can be obtained as follows:

$$\tau_m = K_t i_q - J_m\dot{\omega}_r - B_m\omega_r, \tag{12}$$

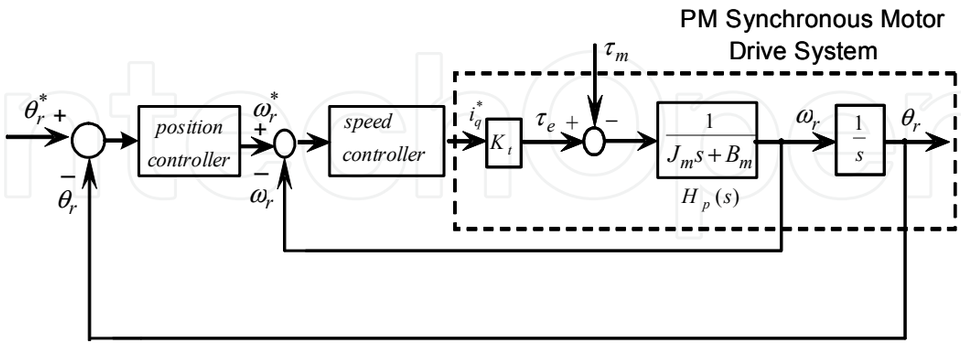

Fig. 2. A simplified control block diagram.

3. Design of the vision-based controllers

The control strategies are to use the non contact measurement CCD as the feedback sensor and design the controller to control the output status of the mechatronic system. Based on

the CCD vision, we will propose the adaptive controller, slider mode controller and fuzzy controller for the mechatronic system. Because the dynamic formulation is obtained, we can perform the controllers in the mechanism modeling numerically, and realize the proposed controllers experimentally.

3.1 Design of an adaptive vision-based controller

The block diagram of the adaptive vision-based control system is shown in Fig. 3, where x_B^*, x_B and θ_1 are the slider command position, slider position and the rotation angle of link 1 of the motor-mechanism system, respectively. The slider position x_B is the desired control objective and can be manipulated from the rotation angle θ_1 by the relation $x_B = 2r_1 \cos\theta_1$, where the angle θ_1 is the experimental measured state by use of a shape pattern in the machine vision system.

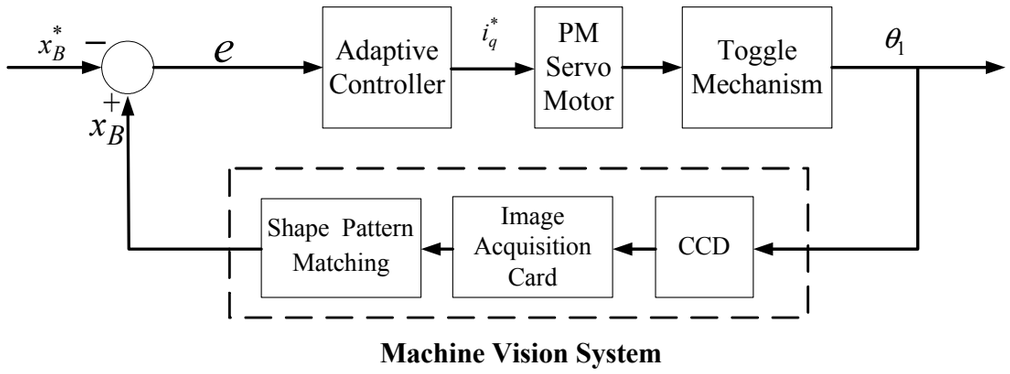

Fig. 3. Block diagram of an adaptive vision-based control system.

In order to design an adaptive control, we rewrite equation (7) as the second-order nonlinear one:

$$U(t) = f(\mathbf{X};t)\ddot{v}(t) + G(\mathbf{X};t) - d(t), \tag{13}$$

where

$$f(\mathbf{X};t) = \hat{\mathbf{Q}}^{-1}\hat{\mathbf{M}},\ G(\mathbf{X};t) = \hat{\mathbf{Q}}^{-1}\hat{\mathbf{N}},\ d(t) = \hat{\mathbf{Q}}^{-1}\hat{\mathbf{D}},$$

and $U(t)$ is the control input current i_q^*. It is assumed that the mass of slider B and the external force F_E are not exactly known. With these uncertainties, the first step in designing an adaptive vision-based controller is to select a Lyapunov function, which is a function of tracking error and the parameters' errors. An inertia-related Lyapunov function (Slotine & Li, 1988; Slotine & Li, 1989; Lin et al., 1997) containing a quadratic form of a linear combination of speed- and position-error states is chosen as follows:

$$V = \frac{1}{2}s^T f(X;t)s + \frac{1}{2}\tilde{\varphi}^T\Gamma^{-1}\tilde{\varphi}, \tag{14}$$

where

$$s = \lambda_e e + \dot{e},\ \ e = x_B - x_B^*,\ \ \Gamma = \begin{bmatrix} \gamma_1 & 0 \\ 0 & \gamma_2 \end{bmatrix},\ \ \tilde{\varphi} = \varphi - \hat{\varphi},\ \ \varphi = \begin{bmatrix} m_B \\ F_E \end{bmatrix},\ \ \hat{\varphi} = \begin{bmatrix} \hat{m}_B \\ \hat{F}_E \end{bmatrix},$$

and λ_e, γ_1 and γ_2 are positive scalar constants. The auxiliary signal s may be considered as a filtered tracking error.
Differentiating Eq. (14) with respect to time gives

$$\dot{V} = s^T f(X;t)\dot{s} + \frac{1}{2} s^T \dot{\hat{Q}}^{-1} \hat{M} s + \frac{1}{2} s^T \hat{Q}^{-1} \dot{\hat{M}} s + \tilde{\varphi}^T \Gamma^{-1} \dot{\tilde{\varphi}}, \tag{15}$$

and multiplying the variable $\dot{s}$ with Eq. (13), we have

$$\begin{aligned} f(X;t)\dot{s} &= f(X;t)(\lambda_e \dot{e} - \ddot{x}_B^* + \ddot{x}_B) \\ &= f(X;t)(\lambda_e \dot{e} - \ddot{x}_B^*) + f(X;t)\ddot{x}_B \\ &= Y(\bullet) + Z(\bullet)\varphi - 2r_1 \sin\theta_1 U, \end{aligned} \tag{16}$$

Substituting Eq. (16) into Eq. (15) gives

$$\begin{aligned} \dot{V} &= s^T (Y(\bullet) + Z(\bullet)\varphi - 2r_1 \sin\theta_1 U) + \frac{1}{2} s^T \dot{\hat{Q}}^{-1} \hat{M} s + \frac{1}{2} s^T \hat{Q}^{-1} \dot{\hat{M}} s + \tilde{\varphi}^T \Gamma^{-1} \dot{\tilde{\varphi}} \\ &\equiv s^T (Y'(\bullet) + Z'(\bullet)\varphi - 2r_1 \sin\theta_1 U) + \tilde{\varphi}^T \Gamma^{-1} \dot{\tilde{\varphi}}, \end{aligned} \tag{17}$$

where $Y(\bullet)$, $Z(\bullet)$, $Y'(\bullet)$ and $Z'(\bullet)$ can be found in (Chuang et al., 2008). If the control input is selected as

$$U = \frac{1}{2r_1 \sin\theta_1} (Y'(\bullet) + Z'(\bullet)\hat{\varphi} + K_V s), \tag{18}$$

where K_V is a positive constant. Eq. (17) becomes

$$\dot{V} = -s^T K_V s + \tilde{\varphi}^T (\Gamma^{-1} \dot{\tilde{\varphi}} + Z'(\bullet)^T s)\,. \tag{19}$$

By selecting the adaptive update rule as

$$\dot{\tilde{\varphi}} = -\dot{\hat{\varphi}} = -\Gamma Z'(\bullet)^T s\,, \tag{20}$$

and substituting into Eq. (19), it then becomes

$$\dot{V} = -s^T K_V s \le 0. \tag{21}$$

As $\dot{V}$ in Eq. (21) is negative semi-definite, then V in Eq. (14) is upper-bounded. As V is upper-bounded and $f(\mathbf{X};t)$ is a positive-definite matrix, i, e, s and $\tilde{\varphi}$ are bounded.
Let function $P(t) = -\dot{V}(t) = s^T K_V s$, and integrate function $P(t)$ with respect to time

$$\int_0^t P(t)dt = V(0) - V(t). \tag{22}$$

Because $V(0)$ is bound, and $V(t)$ is non-increasing and bounded, then

$$\lim_{t\to\infty}\int_0^t P(\tau)d\tau < \infty \,. \tag{23}$$

Differentiate $P(t)$ with respect to time, we have

$$\dot{P}(t) = s^T K_V \dot{s} + \dot{s}^T K_V s \,. \tag{24}$$

Since K_V, s, and $\dot{s}$ are bounded, $P(t)$ is uniformly continuous. From the above description, Barbalat's Lemma (Narendra & Annaswamy, 1988) can be used to state that

$$\lim_{t\to\infty} P(t) = 0. \tag{25}$$

Therefore, it can be obtained as follows

$$\lim_{t\to\infty} s = 0. \tag{26}$$

As a result, the system is asymptotically stable. Moreover, the tracking error of the system will converge to zero according to $s = \lambda_e e + \dot{e}$.

3.2 Design of a sliding mode controller

Rewriting Eq. (7) as a second-order nonlinear, single-input-single-output (SISO) motor-mechanism coupled system as follows:

$$\ddot{v}(t) = f(\mathbf{X};\, t) + G(\mathbf{X};\, t)U(t) + d(t) \tag{27}$$

where

$$f(\mathbf{X};t) = -\hat{M}^{-1}\hat{N} \quad G(\mathbf{X};t) = \hat{M}^{-1}\hat{Q} \quad d(t) = \hat{M}^{-1}\hat{D}$$

and $U(t)$ is the control input v_q^*. It is assumed that the function f is not exactly known, but the extent of the imprecision Δf is bounded by a known continuous function $F(\mathbf{X};\, t)$. Similarly, the control gain $G(\mathbf{X};\, t)$ is not exactly known but having a constant sign and known bounds, *i.e.*

$$0 < G_{\min} \le G(\mathbf{X};\, t) \le G_{\max}. \tag{28}$$

Disturbance $d(t)$ is unknown, but is bounded by a known continuous function $D(\mathbf{X};\, t)$. According to the above descriptions, we have

$$\left| f - \hat{f} \right| \le F(\mathbf{X};\, t) \tag{29a}$$

$$\frac{1}{\alpha} \le \frac{\hat{G}(\mathbf{X};\, t)}{G(\mathbf{X};\, t)} \le \alpha \tag{29b}$$

$$|d| \le D(\mathbf{X};\, t) \tag{29c}$$

where $\hat{f}$ and $\hat{G}$ are nominal values of f and G, respectively, and

$$\alpha = \left(G_{\max}/G_{\min}\right)^{1/2}.$$

The control problem is to find a control law so that the state $\mathbf{X}$ can track the desired trajectory $\mathbf{X}_d$ in the presence of uncertainties.
Let the tracking error vector be

$$\mathbf{e} = \mathbf{X} - \mathbf{X_d} = \left[e\ \dot{e}\right]^T \tag{30}$$

where $\mathbf{X_d} = \left[x_B^*\ \dot{x}_B^*\right]^{\mathbf{T}}$. Define a sliding surface $s(t)$ in the state space R^2 by the scalar function $s(\mathbf{X};t) = 0$, where

$$s(\mathbf{X},\ t) = Ce + \dot{e}\quad C > 0\,. \tag{31}$$

The sliding mode controller is proposed as follows:

$$U = U_{eq} + U_n \tag{32}$$

where

$$U_{eq} = \left(\hat{G}\right)^{-1}\hat{U} \tag{33a}$$

$$U_n = -\left(\hat{G}\right)^{-1} K\,\mathrm{sgn}(s) \tag{33b}$$

and

$$\hat{U} = -\hat{f} - \ddot{v}_d^* + d(t) + C\dot{e} \tag{34}$$

$$K \geq \alpha\left(F + D + \eta\right) + \left(\alpha - 1\right)\left|\hat{U}\right|,\ \mathrm{sgn}(s) = \begin{cases} 1 & if \quad s > 0 \\ 0 & if \quad s = 0 \\ -1 & if \quad s < 0 \end{cases} \tag{35}$$

where η is a positive constant. The detailed derivations of the sliding mode controller are similar to the work of (Slotine & Li, 1992). Some discussions about the sliding mode control could refer to the References (Gao & Hung, 1993; Hung et al., 1993).
To alleviate the chattering phenomenon, we adopt the quasi-linear mode controller (Slotine & Li, 1992), which replaces the discontinuous control laws of Eq. (33b) by a continuous one and insides a boundary layer around the switching surface. That is, U_n is replaced by

$$U_n = -\left(\hat{G}\right)^{-1} K sat\left(\frac{s}{\varepsilon}\right), \tag{36}$$

where $\varepsilon > 0$ is the width of boundary, and the function of $sat\left(\frac{s}{\varepsilon}\right)$ is defined as

$$sat\left(\frac{s}{\varepsilon}\right)=\begin{cases}1 & if \quad s>\varepsilon\\ \dfrac{s}{\varepsilon} & if \quad -\varepsilon\le s\le\varepsilon\\ -1 & if \quad s<-\varepsilon\end{cases} \tag{37}$$

This leads to tracking within a guaranteed precision ε while allowing the alleviation of the chattering phenomenon. The block diagram of the SMC by use of a machine vision system is shown in Fig. 4, where the tracking error is $e=x_B-x_B^*$ and the output displacements of slider B are measured by a machine vision system, which includes the CCD, image acquisition card and color pattern matching.

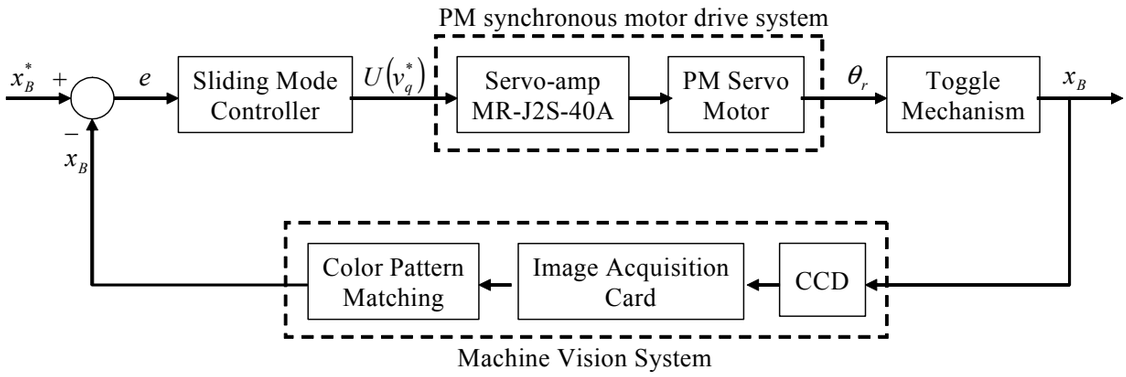

Fig. 4. Block diagram of the sliding mode control by the machine vision system.

3.3 Design of a fuzzy logic controller

In the real situations, the general problem encountered in designing a controller is that the bounds of the uncertainties and exact mathematical models of the motor-toggle mechanism system are difficult to obtain for practical applications. Moreover, the parameters can not be obtained directly and the output responses of slider B must be able to measure. In this chapter, the PD-type FLC (Rahbari & Silva, 2000) and PI-type FLC (Aracil & Gordillo, 2004), which are without using complex mathematical model, are proposed to overcome the difficulties of uncertainties and un-modeling.

3.3.1 The PD-type fuzzy logic controller

The control problem is to find the PD-type FLC law such that the output displacement x_B can track the desired trajectories x_B^* in the presence of uncertainties. Let the tracking error be

$$e=x_B-x_B^* \tag{38}$$

As shown in Fig. 5, the signals of e and $\dot{e}$ are selected as the inputs for the proposed PD-type FLC.

The control output of the PD-type FLC is u, which denotes the change of controller outputs. The signals of e and $\dot{e}$ could be respectively transferred to their corresponding universes of discourse by multiplying scaling factors k_1 and k_2, namely,

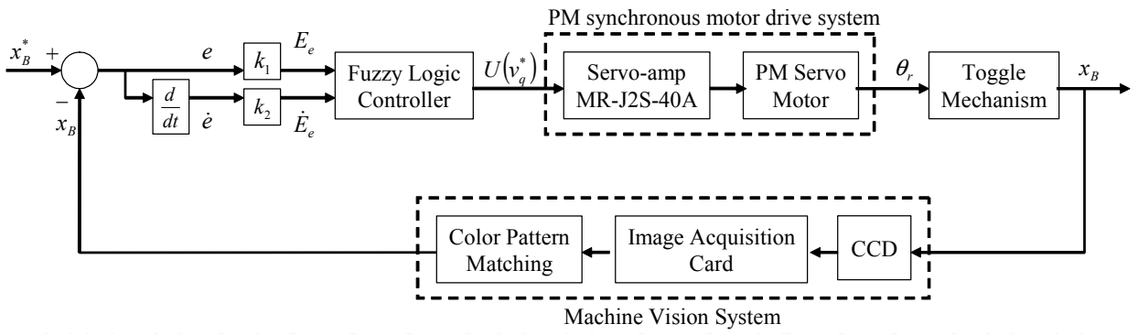

Fig. 5. Block diagram of a PD-type FLC for the motor-toggle mechanism.

$$E_e = e * k_1, \quad E_e = e * k_2 \tag{39}$$

Since the output u of the FLC is in its corresponding universe of discourse, the u could be transferred, by multiplying a scaling factor G_u, to an actual input of the plant, namely,

$$U = u * G_u \tag{40}$$

Because the data manipulation in the PD-type FLC is based on the fuzzy set theory, the associated fuzzy sets involved in the linguistic control rules are defined as follows:

N: Negative *Z*: Zero *P*: Positive
NB: Negative Big *NM*: Negative Medium *NS*: Negative Small
ZE: Zero *PS*: Positive Small *PM*: Positive Medium *PB*: Positive Big

and their universe of discourse are all assigned to be [-10, 10] for a real experimental motor. The membership functions for these fuzzy sets corresponding to E_e, $\dot{E}_e$ and u are defined in Fig. 6.

In the following, the rule bases of the proposed PD-type FLC are systematically constructed on the basis of a Lyapnuov function L_f:

$$L_f = \frac{1}{2}e^2 \geq 0 \text{ and } \dot{L}_f = e\dot{e} \tag{41}$$

According to Lyapnuov stable theory (Cheng & Tzou, 2004), if the system is stable, the conditions $L_f = \frac{1}{2}e^2 \geq 0$ and $e\dot{e} < 0$ are necessary. Therefore, according to Eq. (41), if $e<0$, increasing u will result in decreasing $e\dot{e}$; if $e>0$, decreasing u will result in decreasing $e\dot{e}$. Hence, the control input u can be designed in an attempt to satisfy the condition $e\dot{e} < 0$. The resulting fuzzy control rules are shown in the following:

Rule 1: If E_e is *P* and $\dot{E}_e$ is *P* Then *u* is *NB*

Rule 2: If E_e is *P* and $\dot{E}_e$ is *Z* Then *u* is *NM*

Rule 3: If E_e is *P* and $\dot{E}_e$ is *N* Then *u* is *NM*

Rule 4: If E_e is *Z* and $\dot{E}_e$ is *P* Then *u* is *NS*

Rule 5: If E_e is *Z* and $\dot{E}_e$ is *Z* Then *u* is *ZE*

Rule 6: If E_e is Z and $\dot{E}_e$ is N Then u is PS

Rule 7: If E_e is N and $\dot{E}_e$ is P Then u is PM

Rule 8: If E_e is N and $\dot{E}_e$ is Z Then u is PM

Rule 9: If E_e is N and $\dot{E}_e$ is N Then u is PB.

By using the centre-of-area (COA) method, the output can be obtained as

$$u = \frac{\sum u_k \left[(u_{A_i}(e))(u_{B_j}(\dot{e})) \right]}{\sum ((u_{A_i}(e))(u_{B_j}(\dot{e})))}. \tag{42}$$

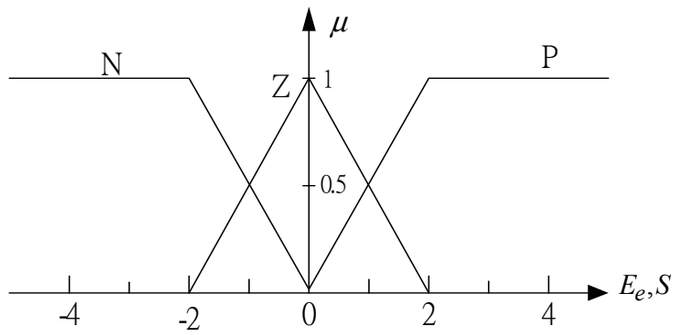

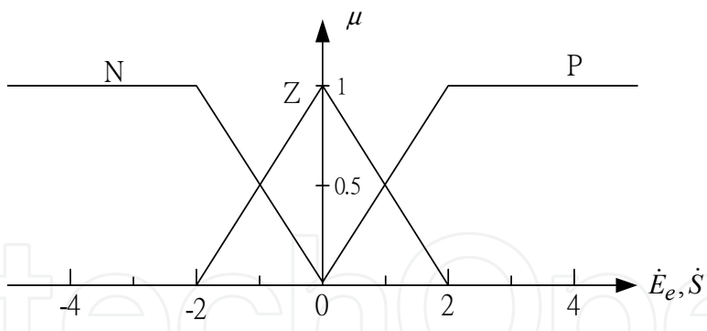

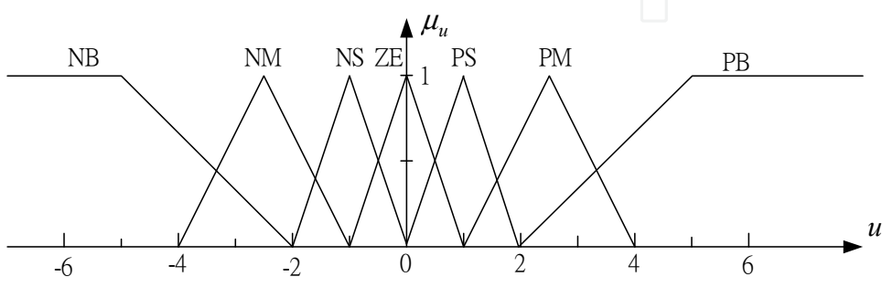

Fig. 6. Membership functions of E_e, S, $\dot{E}_e$, $\dot{S}$ and u.

3.3.2 The PI-type fuzzy logic controller

In this section, the proposed PI-type FLC is designed based on the concept of hitting switch conditions. As shown in Fig. 7, the switching functions are selected as the inputs. In practical implementation, it can be approximated by

$$\dot{s}(kT) = (s(k-1)T) / T \ , \tag{43}$$

where k is the number of iteration and T is the sampling period.

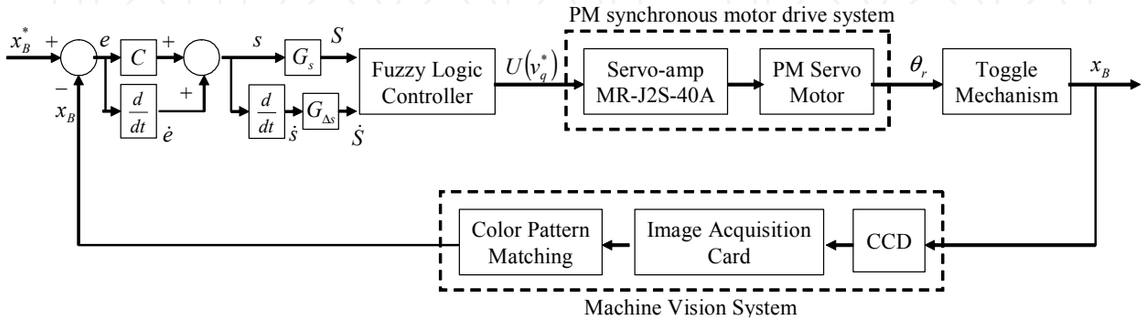

Fig. 7. Block diagram of a PI-type FLC for the motor-toggle mechanism.

The control input of the PI-type FLC is u which denotes the change of the controller outputs. The s and $\dot{s}$ signals could be transferred to their corresponding universes of discourse by multiplying scaling factors G_s and $G_{\Delta s}$ respectively, namely,

$$S = s \cdot G_s, \quad \dot{S} = \dot{s} \cdot G_{\Delta s}. \tag{44}$$

Since the output u of the PI-type FLC is in its corresponding universe of discourse, the u could be transferred, by multiplying a scaling factor $G_{\Delta u}$, to an actual input of the plant, namely,

$$\Delta U = u \cdot G_{\Delta u}. \tag{45}$$

Because the data manipulation in a PI-type FLC is based on fuzzy set theory, the associated fuzzy sets involved in the linguistic control rules are defined as the same as the previous section and their universe of discourse are all assigned the same as the previous section. The membership functions for these fuzzy sets corresponding to S, $\dot{S}$ and u. are also defined in Fig. 6.

In the following, the rule base of the proposed PI-type FLC are systematically constructed on the basis of hitting switching conditions of the SMC. Multiplying of Eq. (43) by s then we have

$$s\dot{s} = fs + GUs + ds - \ddot{v}s + C\dot{e}s. \tag{46}$$

It is similar to the PD-type FLC, Lyapunov function for the PI-type FLC is assigned as $L_f = \frac{1}{2}s^2 \geq 0$. The controller is designed to satisfy the condition $s\dot{s}$ <0, and the whole control system is stable. According to Eq. (44), if s < 0, increasing u will result in decreasing; if s > 0, decreasing u will result in decreasing $s\dot{s}$. Hence, the control input u can be designed in an attempt to satisfy the hitting condition $s\dot{s}$ <0.

The resulting PI-type FLC rules are shown as follows:

Rule 1: If S is P and $\dot{S}$ is P Then u is NB
Rule 2: If S is P and $\dot{S}$ is Z Then u is NM
Rule 3: If S is P and $\dot{S}$ is N Then u is NM
Rule 4: If S is Z and $\dot{S}$ is P Then u is NS
Rule 5: If S is Z and $\dot{S}$ is Z Then u is ZE
Rule 6: If S is Z and $\dot{S}$ is N Then u is PS
Rule 7: If S is N and $\dot{S}$ is P Then u is PM
Rule 8: If S is N and $\dot{S}$ is Z Then u is PM
Rule 9: If S is N and $\dot{S}$ is N Then u is PB.

By using the centre-of-area (COA) method, the output can be obtained as

$$u = \frac{\sum u_k \left[(u_{F_i}(e))(u_{G_j}(\dot{e})) \right]}{\sum ((u_{F_i}(e))(u_{G_j}(\dot{e})))}. \tag{47}$$

In this chapter, the mean of maximum (MOM) of defuzzifier is adopted in both the PD-type and PI-type FLCs.

4. Numerical simulations

For numerical simulations, the parameters of the mechatronic system of the motor-toggle mechanism are chosen as follows:

$m_B = 4.12 \ \text{K}g$, $m_C = 5.58 \ \text{K}g$, $m_2 = 1.82 \ \text{K}g$, $m_3 = 1.61 \ \text{K}g$, $m_5 = 0.95 \ \text{K}g$, $\mu = 0.17$, $r_1 = 0.06 \ m$, $r_2 = 0.032 \ m$, $r_3 = 0.06 \ m$, $r_4 = 0.068 \ m$, $r_5 = 0.03 \ m$, $h = 0.068 \ m$, $\phi = 0.4899 \ rad$, $K_t = 0.5652 \ Nm/A$, $J_m = 6.7 \times 10^{-5} \ Nms^2$, and $B_m = 1.12 \times 10^{-2} Nms/rad$.

The above known parameters are to substitute into Eq. (7), and the system becomes an initial value problem and can be integrated by using the fourth-order Runge-Kutta method with time step $\Delta t = 0.001$ sec and tolerance error 10^{-9}. The control objective is to control the position of slider B to move from the left side to the right side. The initial position is 0.06 m, the desired position is 0.1 m, and the controlled stroke of the slider B is equal to $\Delta x_B = 0.04 \ m$.

4.1 Numerical simulations of adaptive controller

For numerical simulations, the external disturbance force F_E will be added to test the robustness of the adaptive controller. The gains of the adaptive control law (18) are given as follows: $\lambda_e = 10$, $K_V = 194$, $\gamma_1 = 248$ *and* $\gamma_2 = 173$. They are chosen to achieve the best transient performance in the limitation of control effort and the requirement of stability. In the real system, the angles of θ_1, θ_2, and θ_5 are limited in the following ranges: $23^\circ < \theta_1 < 63^\circ$, $325^\circ < \theta_2 < 350^\circ$, and $145^\circ < \theta_5 < 170^\circ$. Therefore, the invertible property of $\hat{\mathbf{Q}}^{-1}$ can be guaranteed and the system function $f(\mathbf{X};t) = \hat{\mathbf{Q}}^{-1}\hat{\mathbf{M}} > 0$ can be proved.

The dynamic responses of slider B and the control efforts i_q^* with and without external disturbance force are compared in Figs. 8(a) and 8(b), respectively. The dotted lines are the desired positions, the dash lines are the transient responses of numerical simulations with external disturbance force F_E = 0 *Nt* and the solid lines are for F_E = -100 *Nt*. The negative sign in the external disturbance force indicates the action direction is opposite to the X-direction in Fig. 1(a). In Fig. 8(a), the transient responses are almost the same and are stable after 0.5 sec and the steady-state error is about 1×10^{-5} *m*. Since the transient responses are almost the same in the presence of uncertainties, it shows the proposed adaptive control is robust. In Fig. 8(b), the maximum control effort $i_q^* = 0.218A$ for $F_E = 0$ *Nt* is smaller than that $i_q^* = 0.710A$ for F_E = -100 *Nt*.

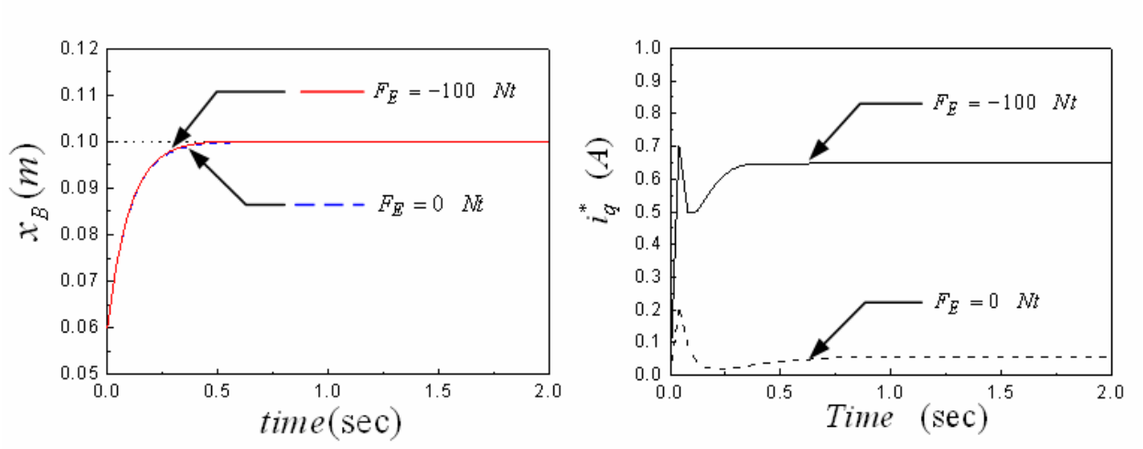

(a) (b)

Fig. 8. The numerical simulations of a motor-toggle mechanism by an adaptive controller with and without external disturbance forces. (a) The dynamic responses of the slider B. (b) The control efforts i_q^*.

4.2 Numerical simulations of sliding mode controller

The nominal case is the system without external disturbance force, i.e., $F_E = 0$ *Nt* and the gains of the SMC are given as C=5 and $\varepsilon = 0.3$. The dynamic responses of slider B for the nominal case are shown in Fig. 9 (a), and it is seen that the response is stable after 1 sec, and the numerical error is about 0.01mm. The trajectories in the phase plane (e, ė) are shown in Fig. 9 (b), where the representative point lies on the designed sliding surface after it hits the switching hyperplane.

Another case with external disturbance force F_E = 100 *Nt* is also considered and the simulation results are shown in Figs. 10(a) and 10(b) for its dynamic responses and trajectories, respectively. It is found that the smooth step-command tracking responses are also obtained well and the SMC is robust to the presence of uncertainties.

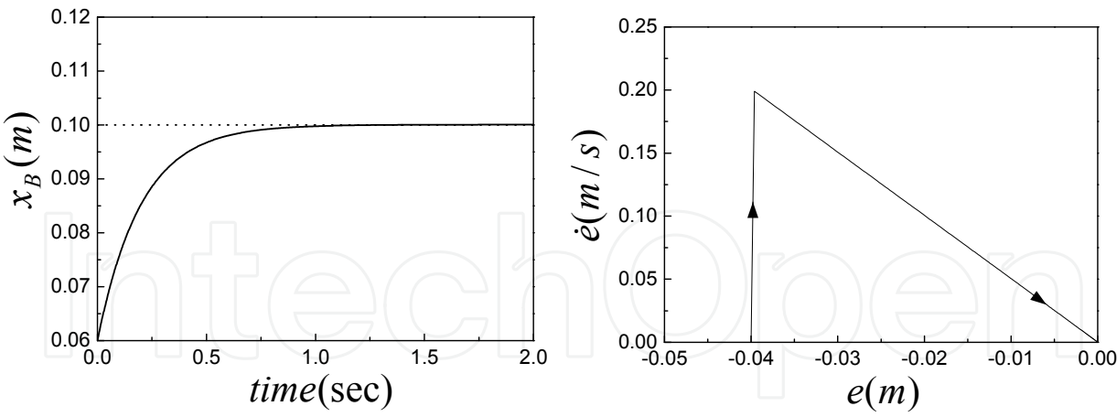

(a) (b)

Fig. 9. (a) The dynamic responses of slider B by the SMC with $F_E = 0 \quad Nt$;
(b) The trajectories in the phase plane by the SMC with $F_E = 0 \quad Nt$.

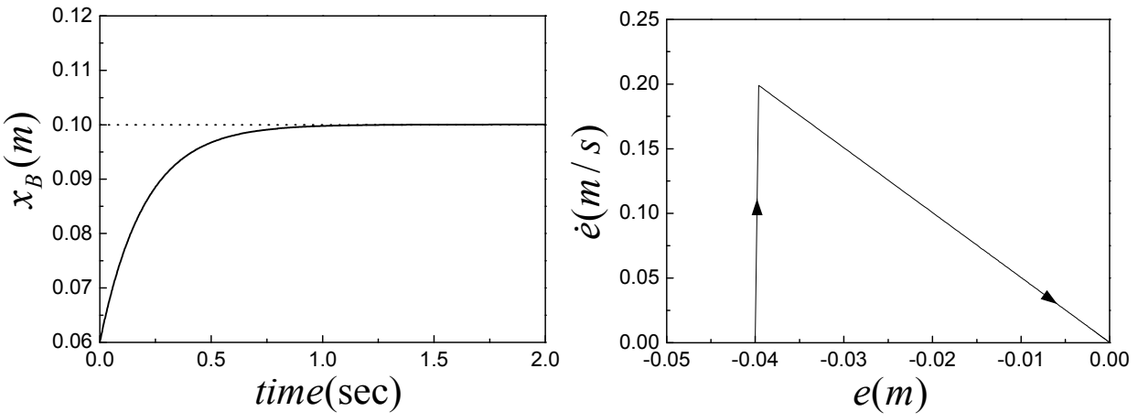

(a) (b)

Fig. 10. (a) The dynamic responses of slider B by the SMC with $F_E = 100 \quad Nt$;
(b)The trajectories in the phase plane by the SMC with $F_E = 100 \quad Nt$.

4.3 Numerical simulations of the PD-type fuzzy logic controller

Here, the PD-type FLC is applied to control the motor-toggle mechanism system numerically. In order to minimize the hitting time and track stable, the scaling factors are determined by observing numerical simulations and are selected as $k_1 = 1082$, $k_2 = 849$ and $G_u = 0.5$. Simulation results of the nominal case without external disturbance force are shown in Fig. 11(a), where the dynamic responses are stable after 1.25 sec, and the error between the desired position and numerical response of slider B is about 0.3 mm. Figure 11(b) illustrates the dynamic responses of the case with external disturbance force F_E = 100 *Nt*. It is seen that the responses are stable after 1.25 sec and the error is about 0.5 mm.

In conclusion, the responses of the PD-type FLC for a motor-toggle mechanism exhibit overshoot phenomenon, and the affection of external disturbance forces to the system is influenced. Therefore, the performance of the proposed PD-type FLC is not robust.

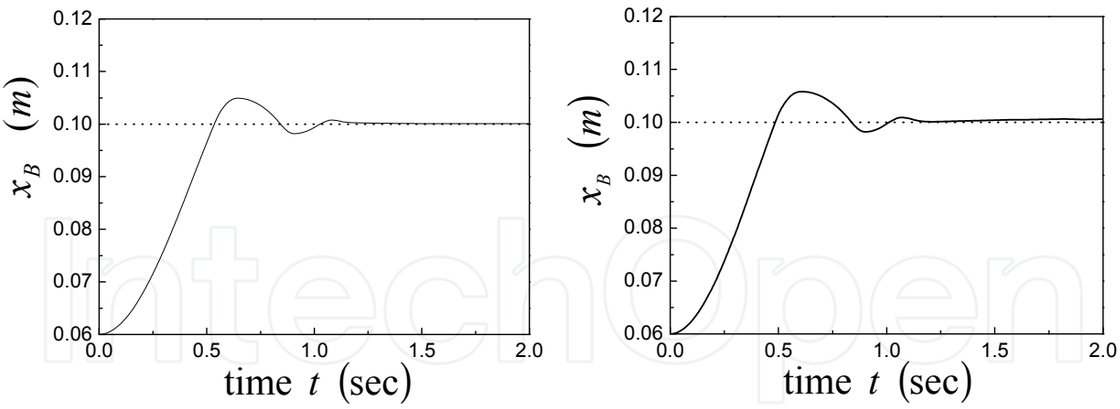

Fig. 11. The dynamic responses of slider B by the PD-type FLC: (a) $F_E = 0 \quad Nt$; (b) $F_E = 100 \quad Nt$.

4.4 Numerical simulations of the PI-type fuzzy logic controller

In this section, the PI-type FLC is applied to control the system numerically and compares with the PD-type FLC. The scaling factors are also determined by observing the numerical simulations, and are selected as:

$$\begin{cases} G_s = 374 \\ G_{\Delta s} = 54 \\ G_u = 0.05 \times |s|^{0.25} \end{cases} \quad if \quad s \geq -0.01, \tag{48}$$

$$\begin{cases} G_s = 534 \\ G_{\Delta s} = 84 \\ G_u = 0.08 \times |s|^{0.25} \end{cases} \quad if \quad s < -0.01. \tag{49}$$

First, the simulation results of the nominal case without external disturbance force are given in Fig. 12(a), where the responses of slider B are stable after 1 sec and the error between the desired position and numerical response is about 0.3 mm. It is noted that the control input is adjusted by the fuzzy inference mechanism, which is based on the concept of hitting conditions regardless of the exact mathematical model. Figure 12(b) illustrates the trajectories in the phase plane. It is seen that the representative point lies on the designed sliding surface $s = 0$ after it hits the switching hyperplane, and the smooth step-command tracking responses are obtained for x_B. Figures 13 (a) and (b) respectively show the trajectories in the phase plane for the system without and with external disturbance force $F_E = 100 \quad Nt$.

In conclusion, the dynamic responses utilizing the PI-type FLC to a motor-toggle mechanism system has no overshoot phenomenon and are stable fast with external force. Furthermore, the PI-type fuzzy controlled motor-toggle mechanism system is robust with respect to the external disturbance forces.

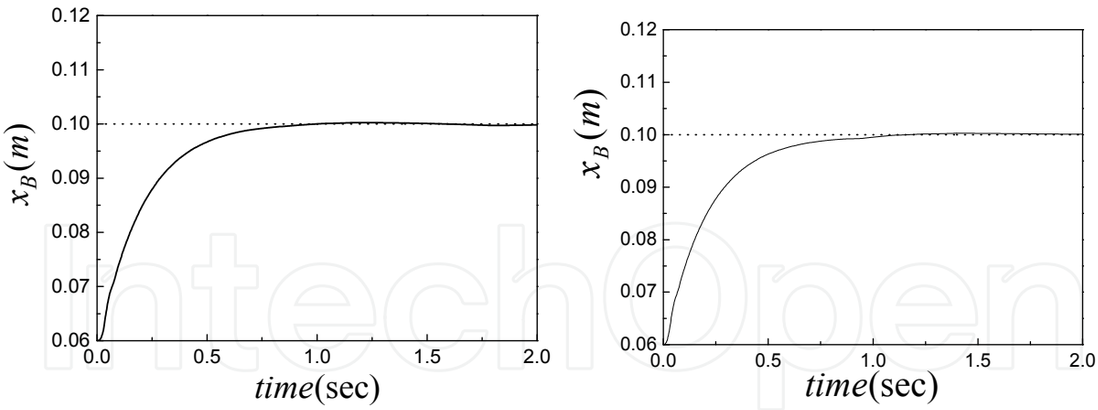

Fig. 12. The dynamic responses of slider B by the PI-type FLC: (a) $F_E = 0 \quad Nt$;
(b) $F_E = 100 \quad Nt$

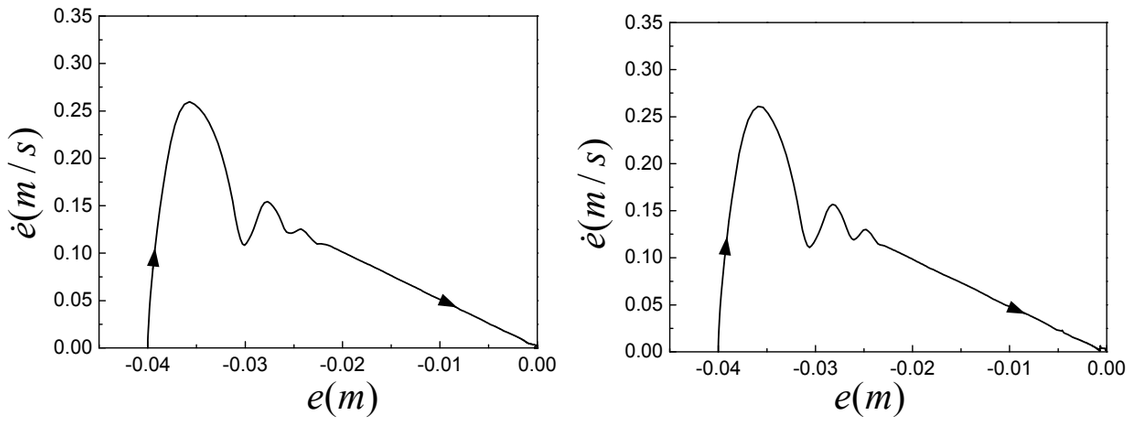

Fig. 13. The trajectories in the phase plane by the PI-type FLC: (a) $F_E = 0 \quad Nt$;
(b) $F_E = 100 \quad Nt$

5. Experiments

In the real operations of an experimental system, the main merit of this study is that the machine vision system of a digital CCD camera is employed as an unconstrained feedback sensor. In Fig. 14(a), the slider position can be measured by non-contacted equipments and a color pattern is pasted to measure and vision-based control. In Fig. 14(b), the state angle θ_1 of the motor-toggle mechanism system is difficult to be measured by an installed encoder and will be experimentally measured by a shape pattern of the machine vision system, which is needed only to paste a pattern on where want to be measured and can be controlled to the desired position by a digital CCD camera.

5.1 Visual control system

The machine vision servoing system takes a color-pattern and a shape-pattern is pasted up on the link and is shown in Fig. 14. It has the advantage in distinguishing the link from its

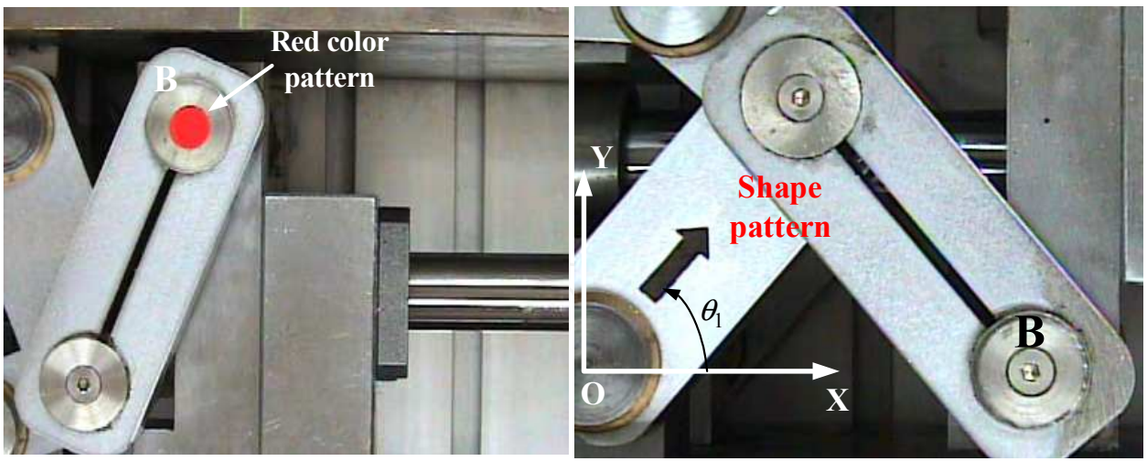

(a) The color pattern (b) The shape pattern

Fig. 14. The control image frame with (a) the color pattern and (b) the shape pattern.

near monotonic surrounding fast. The directional shape pattern is easy identified with measuring the angle θ_1 of the motor-mechanism system. In this vision system, one full-frame of image consists of 752×582 pixels. Searching the whole video data of a full-frame for the shape pattern usually takes quite long time, and degrades the performance of the visual servoing system. Thus, based on the range of the angle θ_1, the image frame is adjusted by a CCD camera to contain the controlled degree of the angle θ_1. Before using the machine vision system, it is very important to do a calibration between one pixel and a real-word unit such as millimeter (mm). Therefore, a standard calibration grid is shown in Fig.15. The real distance in the standard calibration grid of one block point center to another one point center is measured 7 mm in both the X- and Y-directions. The result of calibration is that one pixel is 0.2 mm in the real world. According to this the color pattern image coordinate can be transformed into a real-world unit in designing a control algorithm.

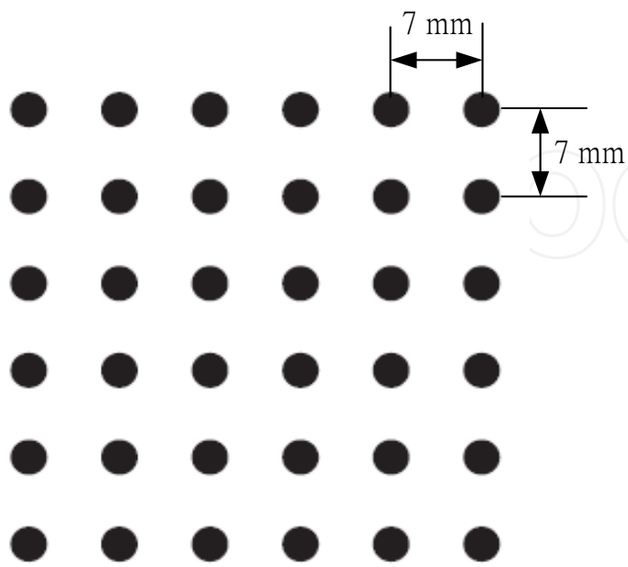

Fig. 15. The standard calibration grid.

After the experimental calibration, pattern matching is the first step for implementing the machine vision system. The servoing control algorithm is implemented by LabVIEW and the image acquisition card is implemented by PCI 1405. In the controlled image frame, the shape pattern is selected as the region of interest (ROI) to save in a disk for searching. Finally, the shape pattern and color pattern matching algorithm is realized by LabVIEW and the position of slider B is controlled by the visual controller. In this study, the image processing time is 0.2 sec by using the CCD camera to feedback the slider position.

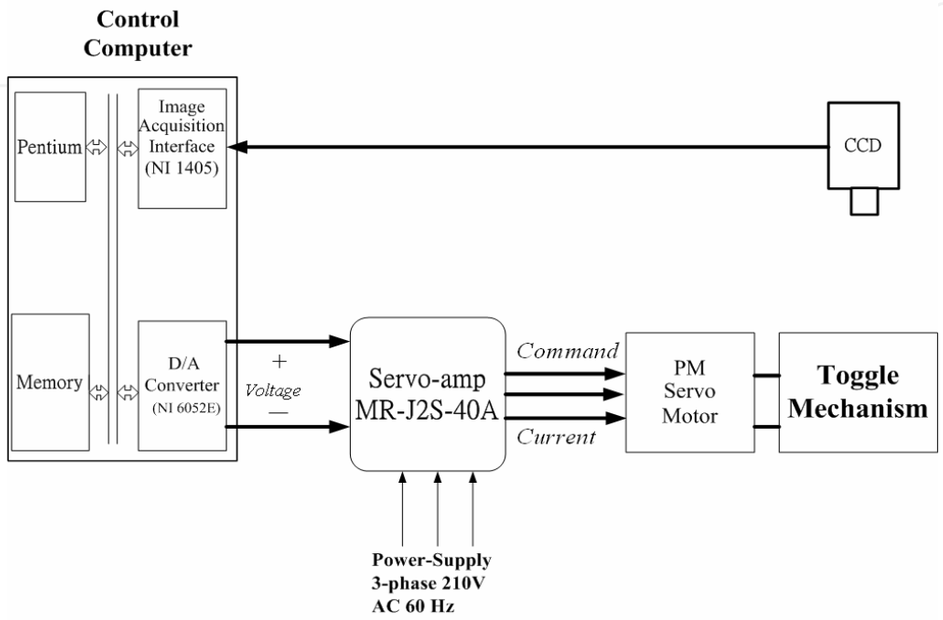

(a)

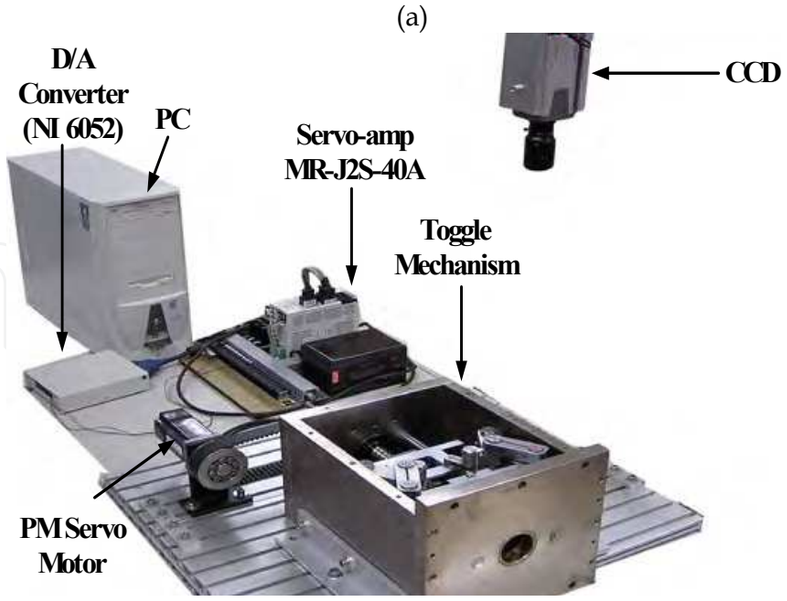

(b)

Fig. 16. The visual control system. (a) The computer control block diagram.
(b) The experimental equipments.

5.2 Experimental setup

The visual control block diagram of the motor-toggle mechanism is shown in Fig. 16(a) and its experimental equipments are shown in Fig. 16(b). The control algorithm is implemented by using a Pentium computer and the control software is LabVIEW. The PMSM is implemented by the MITSUBISHI HC-KFS43 series. The specifications are described as follows: rated output 400 (W), rated torque 1.3 (Nm), rated rotation speed 3000 (rpm) and rated current 2.3 (A). The servo is implemented by the MITSUBISHI MR-J2S-40A1. The control system is a sine-wave PWM control, which is a current control system. The digital CCD camera is implemented by the SONY SSC-DC393 series. The specifications are imaging device 1/3-type interline transfer, picture elements 752(horizontal) ×582(vertical), and Lent CS-mount.

6. Experimental results

6.1 The vision-based adaptive controller

The adaptive vision-based control for the motor-mechanism system is performed by comparing the external disturbance force $F_E = 0 \ \ Nt$ with $F_E = -10 \ \ Nt$. The experimental results of the measured angle θ_1 via the machine vision system, the transient responses of slider B via the manipulating relation $x_B = 2r_1 \cos\theta_1$ and the control efforts i_q^* are shown in Figs. 17-18, respectively. It is seen that the experimentally measured angle θ_1 in Fig. 17 and the transient responses of slider B in Fig.18 are almost the same for the system with and without F_E, and are stable after 0.75 sec. However, the control efforts i_q^* are quite different. The maximum control effort $i_q^* = 0.28A$ for $F_E = 0 \ \ Nt$ is much smaller than that $i_q^* = 0.75A$ for $F_E = -10 \ \ Nt$. The maximum control efforts are near to those of numerical simulations.
Moreover, in order to demonstrate the robust control performance of the adaptive vision-based controller, the experiments are performed by suddenly adding an extra mass 10 kg on slider B at 0.6 sec, and suddenly adding 10 *Nt*of the external force at 0.6 sec. Figure 19(a) show the good performance of regulation problems, and Figure 19(b) show the control input efforts, where the jumps occurs when the extra mass and external force are suddenly added.

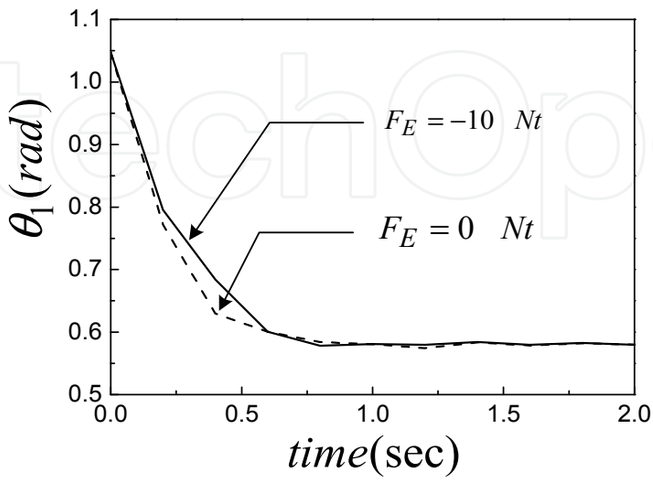

Fig. 17. The experimentally measured angle θ_1 with and without external disturbance forces.

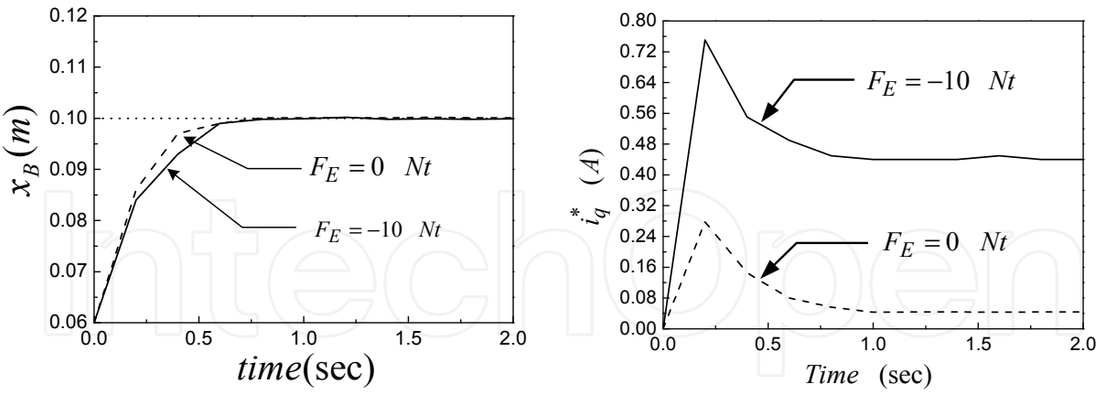

(a) (b)

Fig. 18. (a) The experimentally dynamic responses of slider B with and without external disturbance forces; (b) The experimental control efforts i_q^*

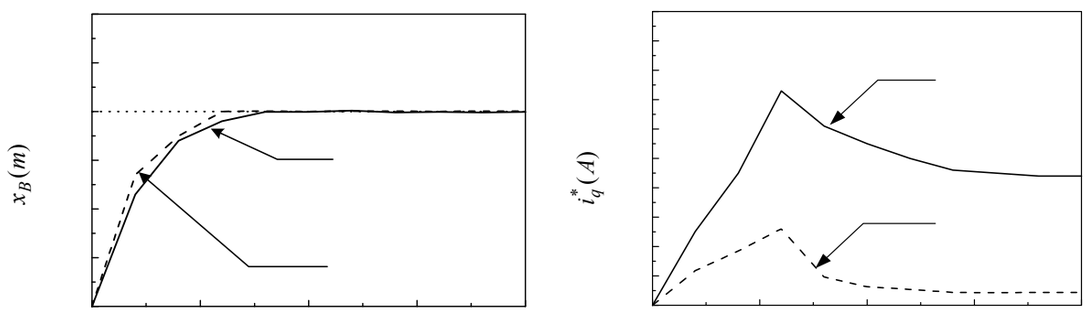

(a) (b)

Fig. 19. (a)The experimentally dynamic responses of slider B with the time-varying external force and mass variation at slider B. (b) Control input efforts with the time-varying external force and mass variation at slider B

6.2 The vision-based sliding mode and fuzzy logic controller

The experiments are performed by suddenly adding an extra mass 10 kg on slider B at 0.6 sec, and suddenly adding 10 Nt force of the external force at 0.6 sec. The initial state is $x_B(0) = 0.06 \quad m$ while the desired position is $x_B^* = 0.1\ m$. The SMC, PD-type FLC and PI-type FLC are performed for the cases with external disturbance forces $F_E = 0 \quad Nt$ and $F_E = 10 \quad Nt$. Some experimental results are provided to demonstrate the effectiveness of the proposed controllers by the machine vision system. First, the SMC is applied to control the motor-toggle mechanism system and the experimentally controlled responses of slider B without and with external disturbance forces are shown in Fig. 20. It is seen that the experimental responses of slider B are all stable after 1 sec and the errors between the desired position and experimental one are about 1 mm. The results show that the smooth step-command responses are obtained for the slider B due to the robust control characteristics of the SMC.

Furthermore, the results via the PD-type and PI-type FLC are compared without and with external disturbance force in Figs. 21(a) and 21(b), respectively. It is seen that the PI-type FLC performance is always superior to PD-type FLC for the system without and with the external disturbance forces. Finally, the control current inputs of the PD-type and PI-type FLCs with and without external disturbance forces are respectively shown in Figs 22(a) and 22(b).

In conclusions of the experiments, the general problems encountered in designing controllers are that the bounds of uncertainties and the exact mathematical models of a motor-mechanism system are difficult to obtain in advance for practical applications. Moreover, the parameters of the motor-mechanism system can not be obtained directly and the output responses must be measured without constraint. From the experimental results, the PI-type FLC owns more robust control characteristics for the motor-mechanism system by using machine vision.

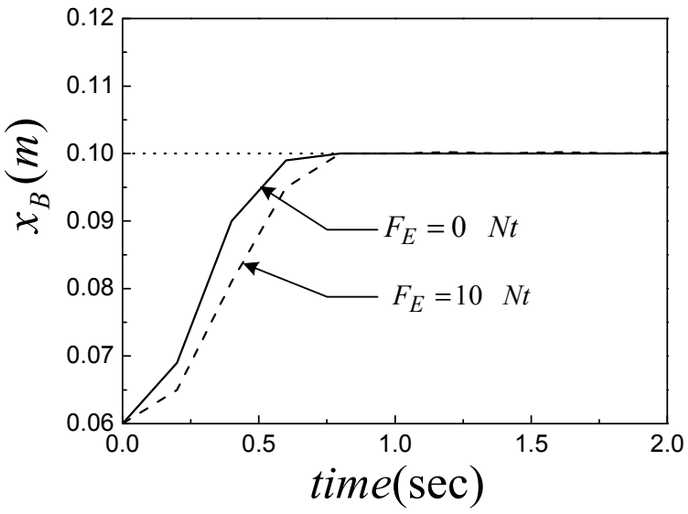

Fig. 20. The experimentally dynamic responses of slider B by the SMC.

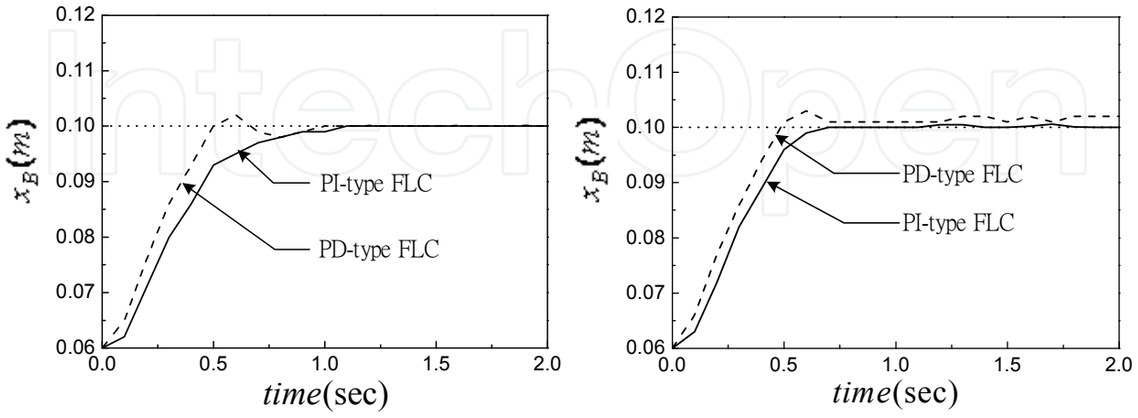

Fig. 21. The experimentally dynamic responses by the PI-type and PD-type FLCs (a) with $F_E = 0\,Nt$; (b) with $F_E = 10 \quad Nt$.

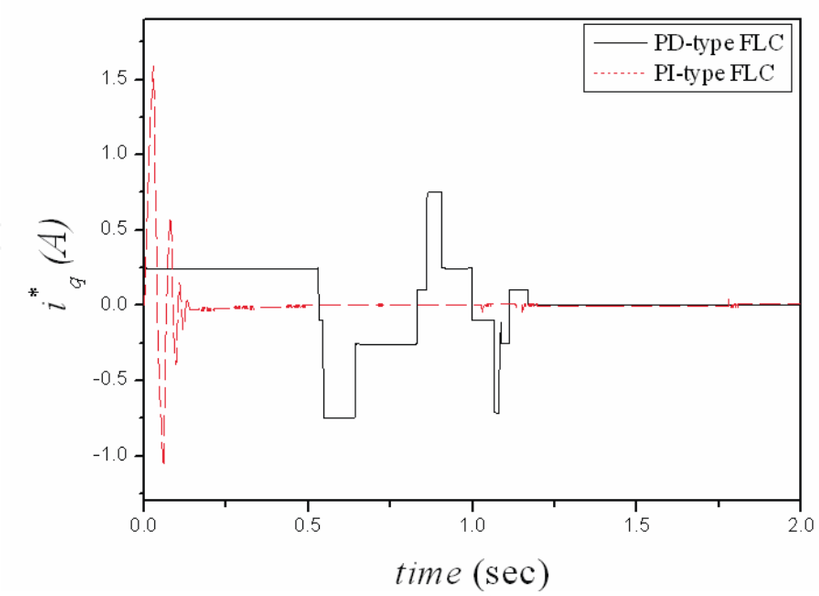

(a)

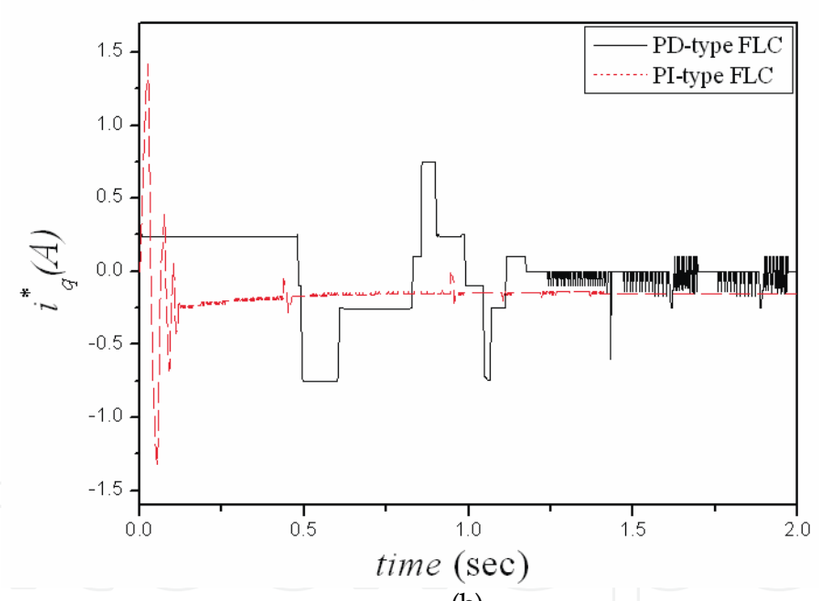

(b)

Fig. 22. The control currents of the PD-type and PI-type FLCs with and without external disturbance forces: (a) The disturbance forces $F_E = 0 \quad Nt$. (b) The disturbance forces $F_E = 10 \quad Nt$.

7. Conclusions

In this chapter, we successfully demonstrate the applications of the proposed adaptive, sliding mode and fuzzy logic vision-based controller to position control of the motor-toggle mechanism system, which is made up by the toggle mechanism driven by a field-oriented

PMSM. In order to overcome the general difficulties of non-contact measuring and external-force uncertainties of the system, the shape pattern and color pattern are designed to measure the rotating angle and slider position, respectively. Finally, the numerical simulations and experimental results are provided to demonstrate the robust control performance of the proposed vision-based controllers.

The main contributions of this study are summarized as:

1. We developed a complete mathematical model for the mechatronic system, which is made up by the toggle mechanism driven by a PMSM.
2. We successfully employed the controllers by machine vision to control the slider position of a complex motor-mechanism coupled system with a simple rule base instead of its complex mathematical model. Moreover, the robust control performance of the mechatronic system is presented with external disturbance forces numerically and experimentally.
3. The color-pattern and shape-pattern matching method of the machine vision are implemented successfully for the mechatronic system. It is shown that the applications of machine vision for industrial equipments are convenient, low cost and multi-useful.

8. References

J. Aracil and F. Gordillo (2004). Describing function method for stability analysis of PD and PI fuzzy controllers. *Fuzzy Sets and Systems* 143, 233-249.

K. Astrom and B. Wittenmark, (1995) *Adaptive control*, Reading. Addison-Wesley, MA.

L. Beji and Y. Bestaoui. (2005). Motion generation and adaptive control method of automated guided vehicles in road following. *IEEE TRANSACTIONS ON INTELLIGENT TRANSPORTATION SYSTEMS 6 (1) 113-123.*

K. Y. Cheng and Y. Y. Tzou, (2004). Fuzzy optimization techniques applies to the design of a digital PMSM servo drive. *IEEE Trans. On Power Electronics* 19, 1085-1099.

C. W. Chuang, M. S. Huang, K. Y. Chen, R. F. Fung. (2008), Adaptive vision-based control of a motor-toggle mechanism: Simulations and experiments. *Journal of Sound and Vibration, 312, 848–861*

R. F. Fung and R. T. Yang (2001). Motion control of an electrohydraulic actuated toggle mechanism. *Mechatronics,* 11, 939-946.

R. F. Fung, J. W. Wu and D. S. Chen. (2001). A variable structure control toggle mechanism driven by linear synchronous motor with joint coulomb friction, *Journal of Sound and Vibration,* 247, 741-753.

W. Gao and J. C. Hung, (1993). Variable structure control of nonlinear systems: a new approach.*IEEE Trans. On Industrial Electronics* 40, 45-55.

M. Hashimoto, F. Oba and T. Tomiie (1999). Mobile robot localization using color signboard. *Mechatronics* 9, 633-656.

M. S. Huang, K. Y. Chen, R. F. Fung (2008), Numerical and experimental identifications of a motor-toggle mechanism, *Applied Mathematical Modelling*

J. Y. Hung, W. Gao and J. C. Hung, (1993), Variable structure control. *IEEE Trans. On Industrial Electronics* 40, 2-22.

Y. Ju, S. K. Chang, B. Jong, S. Hong, M. H. Lee and F. Harashima. (2001). Vision based lateral control by yaw rate feedback. *The 27th Annual Conference of the IEEE Industrial Electronics Society* C, 2135-2138.

T. S. Lee, C. H. Lin and F. J. Lin, (2005). An adaptive H_∞ controller design for permanent magnet synchronous motor drives, Control Engineering Practice 13 425-439.

F. J. Lin, R. F. Fung and Y. S. Lin, (1997). Adaptive control of slider-crank mechanism motion: simulations and experiments, *International Journal of Systems Science* 28 1227-1238.

F. J. Lin, R. F. Fung and Y. C. Wang. (1997). Sliding mode and fuzzy control of toggle mechanism using pm synchronous servomotor drive. *IEE Proceedings Control Theory and Applications,* 144, 393-402.

F. J. Lin and R. J. Wai. (2002). Hybrid computed torque controlled motor-toggle servomechanism using fuzzy neural network uncertainty observer. *Neurocomputing,* 48, 403-422.

Z. B. Li, Z. L. Wang and J. F. Li. (2004). A hybrid control scheme of adaptive and variable structure for flexible spacecraft. *Aerospace Science and Technology,* 8, 423-430.

H. T. Moon, H. S. Kim and M. J. Youg (2003). A discrete-time predictive current control for PMSM. *IEEE Trans. On Power Electronics* 18, 464-472.

K. S. Narendra and A. M. Annaswamy, (1988). *Stable Adaptive System*, Prentice-Hall, Englewood Cliffs, NJ,

O. Nasisi and R. Carelli. (2003). Adaptive servo visual robot control, *Robotics and Autonomous Systems,* 43, 51-78.

J. H. Park and Y. J. Lee, (2002). Robust visual servoing for motion control of the ball on a plate. *Mechatronics* 13, 723-738.

I. Petrovic and M. Brezak (2002). Machine vision based control of the ball and beam. *Advanced Motion Control IEEE 7th International workshop* 3-5, 573-577.

R. Rahbari and C. W. D. Silva (2000). Fuzzy logic control of hydraulic system. *Industrial Technology Proceeding of IEEE International Conference* 2, 313-318.

J. J. E. Slotine and W. Li,(1991). *Applied nonlinear control*, Prentice-Hall, Englewood Cliffs, NJ.

J. J. E. Slotine and W. Li, (1988). Adaptive manipulator control a case study, *IEEE Transactions and Automatic Control* 33, 995-1003.

J. J. E. Slotine and W. Li, (1989) Composite Adaptive control of robot manipulators, *Automatica* 25, 509-519.

R. J. Wai, C. H. Lin and F. J. Lin. (2001). Adaptive fuzzy neural network control for motor-toggle servomechanism. *Mechatronics,* 11, 95-117.

R. J Wai. (2003). Robust fuzzy neural network control for nonlinear motor-toggle servomechanism. *Fuzzy sets and systems,* 139, 185-208.

J. Yong, C. S. Kim, J. Bae, S. Hong, M. H. Lee and F. Harashima, (2001). Vision based lateral control by yaw rate feedback. The 27th Annual Conference of the IEEE Industrial Electronics Society C, 2135-2138.

Visual Servoing

Edited by Rong-Fong Fung

ISBN 978-953-307-095-7

Hard cover, 234 pages

Publisher InTech

Published online 01, April, 2010

Published in print edition April, 2010

The goal of this book is to introduce the visional application by excellent researchers in the world currently and offer the knowledge that can also be applied to another field widely. This book collects the main studies about machine vision currently in the world, and has a powerful persuasion in the applications employed in the machine vision. The contents, which demonstrate that the machine vision theory, are realized in different field. For the beginner, it is easy to understand the development in the vision servoing. For engineer, professor and researcher, they can study and learn the chapters, and then employ another application method.

How to reference

In order to correctly reference this scholarly work, feel free to copy and paste the following:

Rong-Fong Fung and Kun-Yung Chen (2010). Vision-Based Control of the Mechatronic System, Visual Servoing, Rong-Fong Fung (Ed.), ISBN: 978-953-307-095-7, InTech, Available from: http://www.intechopen.com/books/visual-servoing/vision-based-control-of-the-mechatronic-system

INTECH
open science | open minds

InTech Europe
University Campus STeP Ri
Slavka Krautzeka 83/A
51000 Rijeka, Croatia
Phone: +385 (51) 770 447
Fax: +385 (51) 686 166
www.intechopen.com

InTech China
Unit 405, Office Block, Hotel Equatorial Shanghai
No.65, Yan An Road (West), Shanghai, 200040, China
中国上海市延安西路65号上海国际贵都大饭店办公楼405单元
Phone: +86-21-62489820
Fax: +86-21-62489821

IntechOpen